# Analysis of end effects in a linear induction motor by the Wiener-Hopf technique

Prof. K. Venkataratnam, B.E., M.Tech., Ph.D., and T.P. Rao, B.E., M.E., Ph.D.

*Indexing term: Induction motors*

**Abstract:** The paper presents a rigorous 2-dimensional analysis of a double-sided linear induction motor, with particular reference to the entry-end and the exit-end effects. The analysis takes into account the discontinuity of the stator winding as well as the discontinuity of the stator iron. The field equations, together with the boundary conditions, constitute a mixed boundary value problem, which is solved by the use of Wiener-Hopf technique (WHT). The results clearly bring out the individual effects of (i) the discontinuity in the winding and (ii) the discontinuity in the iron, as well as the 2-dimensional nature of the field quantities. The analysis is illustrated by applying it to the data of two linear induction motors.

### List of principal symbols

$A_z$ = $z$-component of vector potential
$J_0$ = peak value of linear current density in primary winding, A/m
$2g$ = airgap length, m
$2d$ = thickness of secondary conducting sheet, m
$L$ = length of stator, m
$V_s$ = synchronous speed, m/s
$v$ = velocity of conducting sheet, m/s
$W$ = width of stator, m
$\omega$ = $2\pi f$ = angular frequency of stator supply, rad/s
$k$ = $\pi/\tau$, where $\tau$ is pole pitch in metres
$\sigma$ = conductivity of the secondary sheet, S/m
$A^*$ = $\int_{-\infty}^{\infty} A_z e^{-sx}\,dx$ = double-sided Laplace transform of $A_z$

Symbols such as $f_1$, $f_2$, $\psi_+$, $\psi'_-$, $G_1$, $G_-$, $C_+$ and $C_-$, which are functions of the transform variable $s$, are defined in the text at appropriate places.

$\alpha_n, -\beta_n$ = zeros of $f_1(s, g)$

$\gamma_n, -\delta_n$ = zeros of $f_2(s, g)$

$$G_+^{(R)}(-\delta_n) = \left\{\frac{s+\delta_n}{G_+(s)}\right\} \quad s = -\delta_n$$

$$G_-^{(R)}(\gamma_n) = \{(s-\gamma_n)\,G_-(s)\}_{s=\gamma_n}$$

## 1 Introduction

A vast amount of work has already been carried out by various investigators regarding the end effects in a short-stator linear induction motor. Notable among these are the works of Yamamura [1, 7], Nasar [2, 8, 9] and Dukowicz [3]. In the 1-dimensional analysis given by Yamamura [1], the effects of discontinuity in the stator winding, as well as stator iron, are taken into account. In the 1-dimensional analysis proposed by Nasar [2], the discontinuity in the stator iron is simulated by assuming fictitious reactive current sheets placed on the stator iron beyond the winding length. The 1-dimensional analysis is too much of an approximation, since it completely ignores the tangential component of the flux density in the airgap. On the other hand, in the 2-dimensional analyses proposed by Yamamura [1] and Nasar and Boldea [9], the effect of discontinuity of the stator winding is considered, but the discontinuity in the iron is ignored to make the problem amenable for analytical solution. They have proposed numerical solutions when both the discontinuity of iron and the discontinuity of winding are to be taken into account. Dukowicz [3] has obtained a 2-dimensional solution for the airgap field by simulating the condition of finite iron length by lining up the iron beyond the stator ends by reactive current sheets, but the solution given is valid for short airgap machines only. The analysis presented in this paper does not call for any such simulation, nor is restricted to small airgap machines. The 2-dimensional airgap field with discontinuous stator iron and discontinuous stator winding has been solved directly by applying the Wiener-Hopf technique and the solution obtained gives a greater insight into the end effects as compared to numerical solutions. In the 1-dimensional analysis, the vector potential, as well as flux density, is assumed independent of $y$ (Fig. 1*a*). In other words, the $B_x$ component is completely ignored. In the 2-dimensional analysis, the vector potential and hence the flux density are function of both $x$ and $y$. Thus, the 2-D analysis enables us to calculate both the 'cross gap' and 'along gap' fields.

## 2 Formulation of problem

The model of a double-sided, short primary LIM is shown in Fig. 1*a*. The Cartesian co-ordinate system is chosen with its origin at the midpoint of the secondary sheet at the entry end. The $x$-axis coincides with the central line of the secondary sheet and the $y$-direction is taken normal to the stator iron. The following assumptions are made in the analysis:

(i) The primary winding is replaced by a thin current sheet, with linear current density given by

$$j_{1z} = J_0 e^{(j\omega t - jkx)} \tag{1}$$

where $\omega$ is the angular frequency of the current and $k = \pi/\tau$.

(ii) The stator and the rotor are considered to be infinitely long in the transverse direction ($z$-direction).

(iii) The rotor of finite thickness is placed symmetrically in the airgap with respect to the stator.

(iv) The flux in each stator block leaves or enters that block only through the surface facing the airgap. It is also assumed that the net leakage flux from either of the stator blocks is zero. Each stator block is considered to be infinitely permeable and perfectly laminated.

It follows from assumption (iv) that the vector potential along AB must be a constant, so also the vector potential along CD (Fig. 1*a*). Furthermore, the vector potential at B must be same as the vector potential at C. For convenience, this constant value of the vector potential can be chosen as zero. Along BC, $A_z$ distribution is not known but $\partial A_z/\partial y$ ($= \mu_0 H_x$) is known and is equal to $\mu_0 J_0 e^{j(\omega t - kx)}$.

Paper 2115B (P1), first received 6th October 1980 and in revised form 14th July 1982

Prof. Venkataratnam is with the Department of Electrical Engineering, IIT, Kharagpur, West Bengal, India, and Mr. T.P. Rao is with the Department of Electrical Engineering, Regional Engineering College, Warangal, Andhra Pradesh, India

Assuming the conducting sheet to be moving with a velocity $v$, the current density in the secondary is given by

$$j_{2z} = \sigma(E + V \times B) = -\sigma\left(\frac{\partial A_z}{\partial t} + v\frac{\partial A_z}{\partial x}\right) \quad (2)$$

Finally, $A_z$ should satisfy

$$\frac{\partial^2 A_z}{\partial x^2} + \frac{\partial^2 A_z}{\partial y^2} = 0 \quad (3a)$$

in the airgap region,

$$= \mu_0\sigma\left(\frac{\partial A_z}{\partial t} + v\frac{\partial A_z}{\partial x}\right) \quad (3b)$$

in the rotor region,
with the following boundary conditions:

(i) $A_z = 0$ at $y = g$ for $x < 0$ and $x > L$. (4a)

(ii) $\frac{\partial A_z}{\partial y} = \mu_0 J_0 e^{j(\omega t - kx)}$ at $y = g$ for $0 < x < L$. (4b)

(iii) In the current region of the rotor: (*a*) the flux lines are symmetrical about the $x$-axis, (*b*) at the rotor surface, $B_y$ and $H_x$ are continuous.

This is a 3-part mixed boundary value problem, which can be solved by using WHT only approximately. However, if the stator is sufficiently long, the entry end effects can be ignored at the exit end, and vice versa. The problem, then, can be simplified to a 2-part mixed boundary value problem, paying attention only to either the entry end or the exit end. An exact solution can be obtained for this problem by WHT.

## 2 Solution to vector potential at entry end

Considering only the entry end (Fig. 1*b*), the boundary conditions are as in eqn. 4, when $L \to \infty$.

We can express $A_z$ in the form $A_z = A(x, y)\, e^{j\omega t}$ and define the bilateral Laplace transform of $A$ as

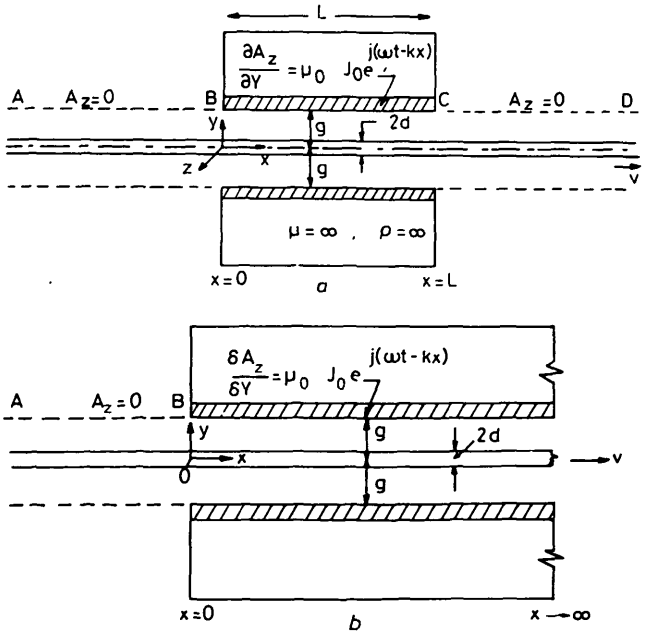


**Fig. 1** *Models of linear induction motor*

*a* Double-sided linear induction motor
*b* Model to study entry-end effect

$$A^*(s, y) = \int_{-\infty}^{+\infty} A(x, y)\, e^{-sx}\, dx$$

The boundary conditions (for $L \to \infty$) could be expressed in terms of $A^*$ as follows:

(i) $A^*(s, g) = \psi_+(s)$, say.

(ii) $\left(\frac{\partial A}{\partial y}\right)^*_{y=g} = \frac{J_0\mu_0}{s + jk} + \psi'_-(s)$.

(iii) (*a*) At $y = 0$, $A_z^*$ is symmetrical at the $x$-axis.

(*b*) At $y = d$, $A_z^*$ and $\frac{\partial A_z^*}{\partial y}$ are continuous.

where

$$\psi_+(s) = \int_0^{\infty} A(x, g)\, e^{-sx}\, dx$$

and

$$\psi'_-(s) = \int_{-\infty}^{0} \left(\frac{\partial A}{\partial y}\right)_{y=g} e^{-sx}\, dx$$

The general solution of eqn. 3 is:

$$A^*(s, y) = P_1 \sin sy + Q_1 \cos sy$$

in the airgap region

$$A^*(s, y) = P_2 \sin \lambda y + Q_2 \cos \lambda y$$

in the rotor, where

$$\lambda^2 = s^2 - v\mu_0\sigma s - j\omega\mu_0\sigma$$

$P_1$, $P_2$, $Q_1$ and $Q_2$ are the constants yet to be obtained. Making use of the boundary conditions and eliminating $P_1, P_2, Q_1, Q_2$, we finally have:

$$\frac{\psi_+(s)}{\psi'_-(s) + \frac{\mu_0 J_0}{(s + jk)}} = \frac{f_1(s, g)}{f_2(s, g)} \quad (5a)$$

where

$$f_1(s, g) = \{\sin sd \cos \lambda d - (\lambda/s) \sin \lambda d \cos sd\} \sin sg + \{\cos sd \cos \lambda d + (\lambda/s) \sin \lambda d \sin sd\} \cos sg \quad (5b)$$

$$f_2(s, g) = \{\sin sd \cos \lambda d - (\lambda/s) \sin \lambda d \cos sd\} s \cos sg - \{\cos sg \cos \lambda d + (\lambda/s) \sin \lambda d \sin sd\} s \sin sg \quad (5c)$$

In eqn. 5, $\psi_+$ and $\psi'_-$ are unknown. The Wiener-Hopf technique attempts to solve these two unknowns from the single equation, eqn. 5, making use of the analytic continuity of $\psi_+$ and $\psi'_-$ and Liouville's theorem. The technique and its applications are extensively discussed by Noble [4] and Collin [5]. When $\psi_+$ and $\psi'_-$ are known, $A^*$ can be obtained. The method of evaluating $\psi_+$ and $\psi'_-$ is given in Section 10.

Making use of the results in Section 10, we finally have:

$$A^* = \left\{\frac{J_0\mu_0}{(s + jk) f_2(s, g)} + \frac{1}{G_+(s) f_1(s, g)} \times \sum_m \frac{J_0\mu_0 G_-^{(R)}(\gamma_m)}{(\gamma_m + jk)(\gamma_m - s)}\right\} f_1(s, y)$$

where

$$G_-^{(R)}(\gamma_m) = \{(s-\gamma_m)G_-\}_{s=\gamma_m}$$

The vector potential $A(x, y)$ is obtained by taking the inverse transform of $A^*$, defined as:

$$A(x, y) \frac{1}{2\pi j} \int_{c-j\infty}^{c+j\infty} A^* e^{sx} ds$$

where $a < c < b$.

This integral is evaluated by making use of Cauchy's residue theorem. For $x > 0$, we choose the contour shown in Fig. 2*a*. This encloses the roots $-jk$, $-\beta_1$, $-\beta_2$ . . . and $-\delta_1$, $-\delta_2$ . . .

Thus we obtain:

$$A(x, y) = \left\{\frac{J_0\mu_0 f_1(s, y) e^{sx}}{f_2(s, g)}\right\}_{s=-jk}$$

$$+ \sum_n \left\{\frac{J_0\mu_0 f_1(s, y) e^{sx}}{(s+jk) f_2'(s, g)}\right\}_{s=-\delta_n}$$

$$+ \sum_n \left[\left\{\frac{f_1(s, y) e^{sx}}{G_+^{(R)}(s) f_1(s, g)}\right\} \times \sum_m \frac{J_0\mu_0 G_-^{(R)}(\gamma_m)}{(\gamma_m + jk)(\gamma_m - s)}\right]_{s=-\delta_n}$$

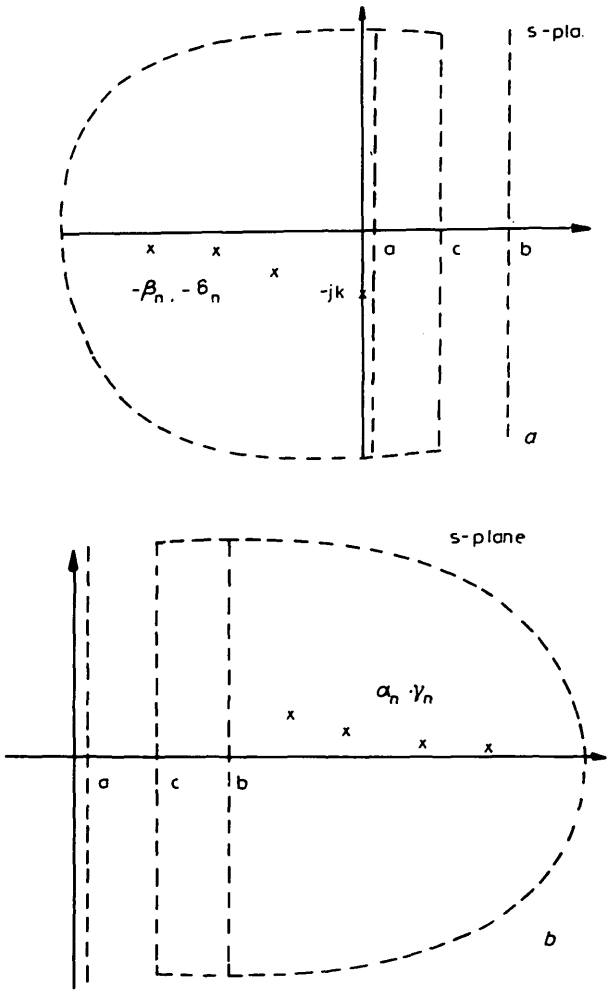


**Fig. 2** *Contours of integration to obtain A(x, y)*

*a* For $x > 0$
*b* For $x < 0$

where

$$G_+^{(R)}(-\delta_n) = \left\{\frac{(s+\delta_n)}{G_+(s)}\right\}_{s=-\delta_n}$$

For $x < 0$, the contour chosen encloses the zeros $\alpha$s and $\gamma$s (Fig. 2*b*), leading to

$$A(x, y) = -\sum_n \left\{\frac{f_1(s, y) e^{sx}}{G_+(s) f_1'(s, g)} \times \sum_m \frac{J_0\mu_0 G_-^{(R)}(\gamma_m)}{(\gamma_m + jk)(\gamma_m - s)}\right\}_{s=\alpha_n}$$

The various quantities $\alpha_n, \beta_n, \gamma_n, \delta_n, G_+^{(R)}, G_-^{(R)}$ are defined in Section 10. $\alpha$s and $-\beta$s are the zeros of $f_1(s, g)$, and $\gamma$s and $-\delta$s are the zeros of $f_2(s, g)$.

## 3 Vector potential at exit end

The exit-end field can be obtained by following a procedure similar to the case of entry end. The origin of the co-ordinate system is shifted to the exit end, as shown in Fig. 3.

The final expression for the vector potential for $x < 0$ is:

$$A(x, y) = \left\{\frac{J_0\mu_0 e^{sx} f_1(s, y)}{f_2(s, g)}\right\}_{s=-jk}$$

$$+ \sum_n \left\{\frac{J_0\mu_0 e^{sx} f_1(s, y)}{(s+jk) f_2'(s, g)}\right\}_{s=\gamma_n}$$

$$+ \sum_n \left[\left\{\frac{J_0\mu_0 G_-^{(R)}(s) e^{sx} f_1(s, y)}{f_1(s, g)}\right\} \times \sum_m \frac{1}{(-\delta_m + jk)(-\delta_m - s) G_+^{(R)}(-\delta_m)}\right]_{s=\gamma_n}$$

For $x > 0$,

$$A(x, y) = -\sum_n \left\{\frac{J_0\mu_0 G_-(s) e^{sx} f_1(s, y)}{f_1'(s, g)} \times \sum_m \frac{1}{(-\delta_m + jk)(-\delta_m - s) G_+^{(R)}(-\delta_m)}\right\}_{s=-\beta_n}$$

## 4 A method of accounting for fringing flux and possible iron extension beyond winding

In the model shown in Fig. 1*a*, the length of the stator iron is taken exactly the same as the winding length and the fringing flux from the end faces of the stator block is neglected. To approximately accommodate the latter, it can be imagined that

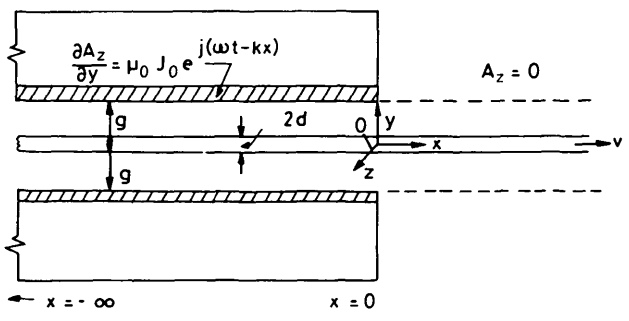


**Fig. 3** *Model for studying exit-end effect*

the stator iron extends beyond the stator winding by a small amount [13], say $L_1$, $L_1$ being chosen so as to keep the permeance of the extended portion equal to the permeance of the fringing flux from the end faces calculated by any suitable method such as conformal mapping. For a stator block of height $h$, the extension $L_1$ is given by the relation

$$\frac{h}{g} = \frac{1}{\pi}\left\{2\sqrt{\exp\left(\frac{\pi L_1}{g}\right) - 1} + \pi - 2\tan^{-1}\sqrt{\exp\left(\frac{\pi L_1}{g}\right) - 1}\right\} \tag{6}$$

$L_1$ may also be made to include any real extension of the stator which is most likely to be present in a practical machine.

With iron extension, the model becomes as shown in Fig. 4*a* at the entry end, and as shown in Fig. 4*b* at the exit end. There will be no difficulty in extending the WHT to solve for $A_z$ for these models also. The relevant expressions for $A_z$ are:

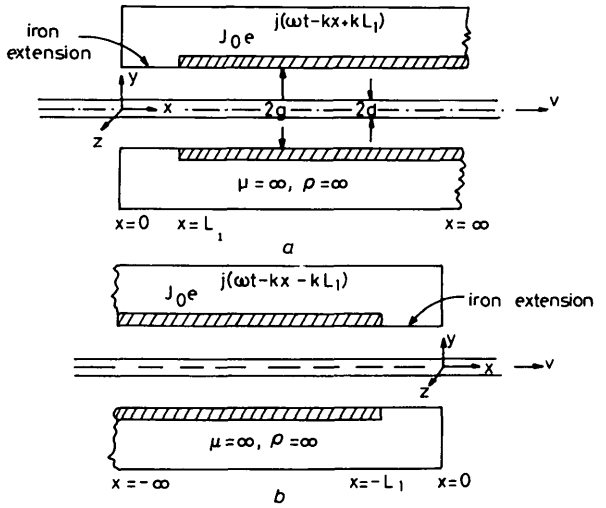


**Fig. 4** *Model of LIM with finite iron extension*
*a* At entry end
*b* At exit end

*At the entry end (Fig. 4a)*

(i) $x < 0$

$$A_z = -\sum_n \left\{ \sum_m \frac{J_0\mu_0 G_-^{(R)}(\gamma_m)e^{-\gamma_m L_1}}{(\gamma_m + jk)(\gamma_m - s)} \frac{f_1(s,y)e^{sx}}{f_1'(s,g)G_+(s)} \right\}_{s=\alpha_n} \tag{7a}$$

(ii) $0 < x < L_1$

$$A_z = -\sum_n \left\{\frac{J_0\mu_0 f_1(s,y)\, e^{s(x-L_1)}}{(s+jk)f_2'(s,g)}\right\}_{s=\gamma_n} + \sum_n \left\{ \sum_m \frac{J_0\mu_0 G_-^{(R)}(\gamma_m)e^{-\gamma_m L_1}}{(\gamma_m + jk)(\gamma_m - s)} \frac{f_1(s,y)e^{sx}}{f_1(s,g)G_+^{(R)}(-\delta_n)} \right\}_{s=-\delta_n} \tag{7b}$$

(iii) $x > L_1$

$$A_z = \left\{\frac{J_0\mu_0 f_1(s,y)e^{s(x-L_1)}}{f_2(s,g)}\right\}_{s=-jk} + \sum_n \left\{\frac{J_0\mu_0 f_1(s,y)e^{s(x-L_1)}}{(s+jk)f_2'(s,g)}\right\}_{s=-\delta_n} + \sum_n \left[ \sum_m \left\{\frac{J_0\mu_0 G_-^{(R)}(\gamma_m)e^{-\gamma_m L_1}}{(\gamma_m + jk)(\gamma_m - s)}\right\} \frac{f_1(s,y)e^{sx}}{G_+^{(R)}(-\delta_n)f_1(s,g)} \right]_{s=-\delta_n} \tag{7c}$$

In eqn. 7*c*, the second and third terms on the RHS represent the effects due to discontinuity in winding and iron, respectively.

*At exit end (Fig. 4b)*

(i) $x > 0$

$$A_z = -\sum_n \left\{ \frac{G_-(s)f_1(s,y)e^{sx}}{f_1'(s,g)} \times \sum_m \frac{J_0\mu_0 e^{-\delta_m L_1}}{(-\delta_m + jk)(-\delta_m - s)G_+^{(R)}(-\delta_m)} \right\}_{s=-\beta_n} \tag{8a}$$

(ii) $-L_1 < x < 0$

$$A_z(x,y) = -\sum_n \left\{\frac{J_0\mu_0 e^{s(x+L_1)}f_1(s,y)}{(s+jk)f_2'(s,g)}\right\}_{s=-\delta_n} + \sum_n \left\{ \frac{G_-^{(R)}(\gamma_n)f_1(s,y)e^{sx}}{f_1(s,g)} \times \sum_m \frac{J_0\mu_0 e^{-\delta_m L_1}}{(-\delta_m + jk)(-\delta_m - s)G_+^{(R)}(-\delta_m)} \right\}_{s=\gamma_n} \tag{8b}$$

(iii) $x < -L_1$

$$A_z(x,y) = \sum_n \left\{\frac{J_0\mu_0 e^{s(x+L_1)}f_1(s,y)}{(s+jk)f_2'(s,g)}\right\}_{s=\gamma_n} + \left\{\frac{J_0\mu_0 e^{s(x+L_1)}f_1(s,y)}{f_2(s,g)}\right\}_{s=-jk} + \sum_n \left\{ \frac{G_-^{(R)}(\gamma_n)e^{sx}f_1(s,y)}{f_1(s,g)} \times \sum_m \frac{J_0\mu_0 e^{-\delta_m L_1}}{(-\delta_m + jk)(-\delta_m - s)G_+^{(R)}(-\delta_m)} \right\}_{s=\gamma_n} \tag{8c}$$

## 5 Expressions for flux density and thrust

### 5.1 Flux density

The expressions given for $A_z$, $B_x$ and $B_y$ can be obtained from the well known relations

$$B_x = \frac{\partial A_z}{\partial y} \quad \text{and} \quad B_y = -\frac{\partial A_z}{\partial x} \tag{9}$$

### 5.2 Thrust

The tractive force is obtained by calculating the reaction on the stator block, using Lorentz equation

$$F = \tfrac{1}{2}\,\mathrm{Re}\int (B_y)_{y=g}\bar{j}_{1z}\,dx$$

where $\bar{j}_{1z}$ = conjugate of $j_{1z}$

$$= \tfrac{1}{2}\,\mathrm{Re}\int\left(-\frac{\partial A_z}{\partial x}\right)_{y=g}\bar{j}_{1z}\,dx \quad \text{N/m} \tag{10}$$

(force per metre width of the stator block)

The integration is to be carried over the winding length. Of the different components of $A_z$, the component due to continuous winding and continuous iron gives rise to a force which is equal to

$$-W\,\mathrm{Re}\left\{\frac{sJ_0^2\mu_0 f_1(s,g)}{f_2(s,g)}\right\}_{s=-jk} \quad \text{N/m} \tag{11}$$

for both the stator blocks. This force is constant per unit length in the $x$-direction and represents the normal induction-motor force.

The remaining terms in $A_z$ contribute to the force due to the end effects. Since these terms decay with the distance from the ends, the total force due to these can be calculated by choosing the limits of integration in eqn. 10 as zero and infinity. Thus, the total force due to entry-end effect

$$\begin{aligned} &= W\,\mathrm{Re}\sum_n\left\{\frac{sJ_0^2\mu_0 f_1(s,g)}{(s+jk)^2 f_2'(s,g)}\right\}_{s=-\delta_n} \\ &+ W\,\mathrm{Re}\sum_n\left\{\frac{sJ_0 e^{sL_1}}{G_+^{(R)}(s)(s+jk)}\times\right. \\ &\left.\sum_m\frac{J_0\mu_0 G_-^{(R)}(\gamma_m)e^{-\gamma_m L_1}}{(\gamma_m+jk)(\gamma_m-s)}\right\}_{s=-\delta_n} \end{aligned} \tag{12}$$

This force is generally negative (except for extremely small values of slip) and hence represents a brake force. Of the two terms in eqn. 12, the first term represents the force due to discontinuity in the winding, and the second term represents the force due to discontinuity in iron.

Similarly, the total force due to the exit end effect

$$\begin{aligned} &= -W\,\mathrm{Re}\sum_n\left\{\frac{sJ_0^2\mu_0 f_1(s,g)}{(s+jk)^2 f_2'(s,g)}\right\}_{s=\gamma_n} \\ &- W\,\mathrm{Re}\sum_n\left\{\frac{sJ_0^2\mu_0 G_-^{(R)}(s)e^{-\gamma_n L_1}}{(s+jk)}\times\right. \\ &\left.\sum_m\frac{e^{-\delta_m L_1}}{(-\delta_m+jk)(-\delta_m-s)G_-^{(R)}(-\delta_m)}\right\}_{s=\gamma_n} \end{aligned} \tag{13}$$

This force is generally positive and hence adds to the thrust. In eqn. 13, the first component is due to the effect of discontinuity in the winding and the second component is due to the discontinuity in iron.

## 6 Applications

To illustrate the nature of flux distribution at the entry end and exit end with different iron extensions (to the stator) and the corresponding end effect force, the data of motor A of Reference 1 are used, as given in the following paragraph.

Number of poles, $P = 4$: frequency = 50 Hz; synchronous speed, $V_s = 9$ m/s; airgap length, $2g = 0.015$ m; secondary (copper) sheet thickness, $2d = 0.005$ m; core length, $L = 0.36$ m; core width, $W = 0.09$ m; peak value of primary current density, $J_0 = 70000$ A/m; conductivity of secondary sheet, $\sigma = 0.59 \times 10^8$ S/m.

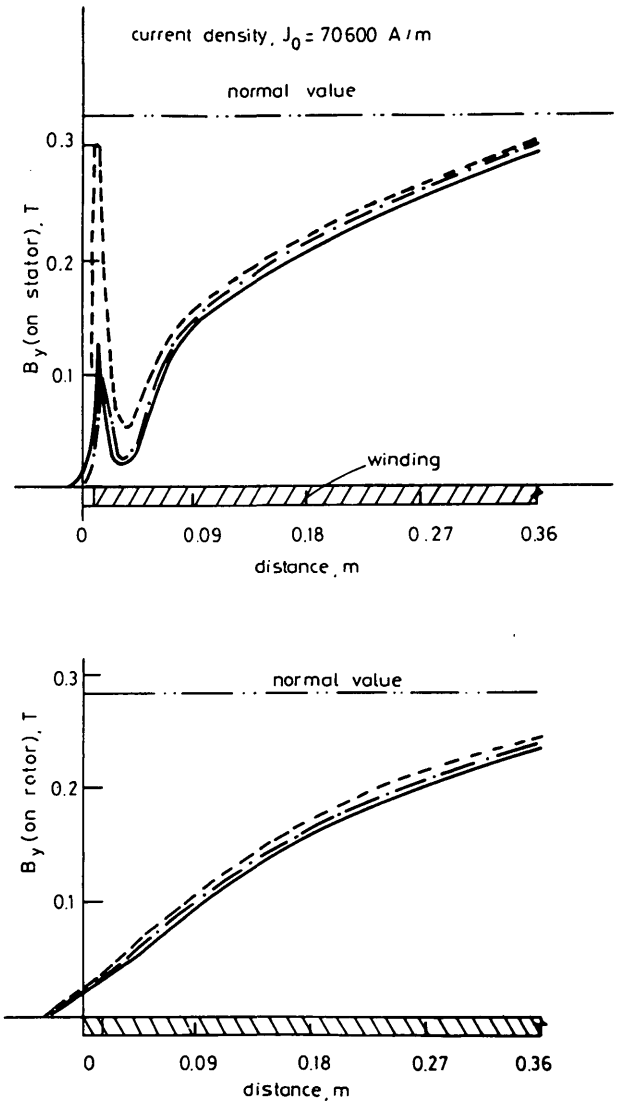


**Fig. 5** *Flux distribution due to entry-end effect (Motor A, 0.05 slip)*
– – – – stator without iron extension
– · – · – stator with a small iron extension (0.0124 m)
——— with infinite iron extension

**Table 1: Zeros of $f_1(s,g)$ and $f_2(s,g)$**

| Motor A, slip 0.05 ($v$ = 8.55 m/s) | | | | |
|---|---|---|---|---|
| $n$ | Roots of $f_1(s,g)$: eqn. 5b | | Roots of $f_2(s,g)$: eqn. 5c | |
| | $\alpha_n$ | $-\beta_n$ | $\gamma_n$ | $-\delta_n$ |
| 1 | 404.3 + j12.7 | −90.6 − j25.9 | 164.2 + j19.6 | −5.8 − j35.5 |
| 2 | 817.9 + j12.1 | −560.9 − j3.1 | 629.1 + j12.3 | −333.0 − j5.2 |
| 3 | 1152.0 + j4.8 | −957.8 − j3.5 | 978.5 + j8.9 | −768.1 − j3.2 |
| 4 | 1582.0 + j2.5 | −1360.0 − j2.5 | 1359.0 + j2.9 | −1152.0 − j3.2 |
| 5 | 2011.0 + j2.6 | −1796.0 − j1.6 | 1803.0 + j2.6 | −1579.0 − j1.9 |
| 6 | 2408.0 + j1.8 | −2206.0 − j1.6 | 2209.0 + j2.3 | −2006.0 − j1.6 |
| 7 | 2834.0 + j1.4 | −2617.0 − j1.3 | 2617.0 + j1.5 | −2409.0 − j1.6 |
| 8 | 3258.0 + j1.4 | −3047.0 − j1.0 | 3049.0 + j1.4 | −2833.0 − j0.12 |

From the preceding data, we obtain $\omega = 314.15$ rad/s, $\tau = 0.09$ m, $k = \pi/\tau = 34.8$. First, the zeros of $f_1(s, g)$ and $f_2(s, g)$ for any chosen value of the slip are to be determined. Choosing a slip of 0.05, $v$ is 8.55 m/s, and, for this value of $v$, Table 1 gives the zeros of $f_1(s, g)$ and $f_2(s, g)$ determined by the Newton-Raphson method.

Next, the $A_z$ distribution can be obtained, using eqns. 7 and 8 and the flux density, and end-effect forces can be determined, using eqns. 9, 12 and 13. Fig. 5 gives the nature of the $B_y$ distribution on the stator and rotor surface due to entry-end effect with different iron extensions to the stator. Fig. 6 gives the corresponding distribution due to exit-end effect.

In a similar way, the $B_y$ distribution obtained on the stator and rotor for a higher value of slip (0.6) are shown in Fig. 7 near the entry end, and in Fig. 8 near the exit end.

The variation of entry-end effect force with slip is shown in Fig. 9, and that of exit-end force in Fig. 10, for different iron extensions to the stator.

The following conclusions can be drawn from the flux-distribution curves:

(i) The 2-dimensional analysis brings out clearly the distinction between the flux distributions on the stator and rotor.

(ii) The entry-end effect, which lasts over considerable distance from the entry end for small values of slip, is mainly due to the discontinuity in the winding. The discontinuity in the iron gives rise to peaking of flux density of the stator in a very short region near the tip of the entry end.

(iii) The exit-end effect, which persists over a relatively short distance at the exit end, is more affected by discontinuity in iron. The discontinuity (in iron) gives rise to a very sharp rise of flux density on the stator surface at the exit end.

(iv) The results for a stator with even a small amount of iron extension (approximately equal to the gap length) are nearly same as those of infinite iron extension.

From the end-effect force curves shown in Figs. 9 and 10, the following conclusions can be drawn:

(i) The entry-end effect force is generally negative (thus reducing the net thrust) except at very small values of slip ($< 0.01$). The discontinuity in iron increases the negative force by a very small amount.

(ii) The exit-end force is generally positive, thus helping the thrust to a small extent. The discontinuity in iron increases

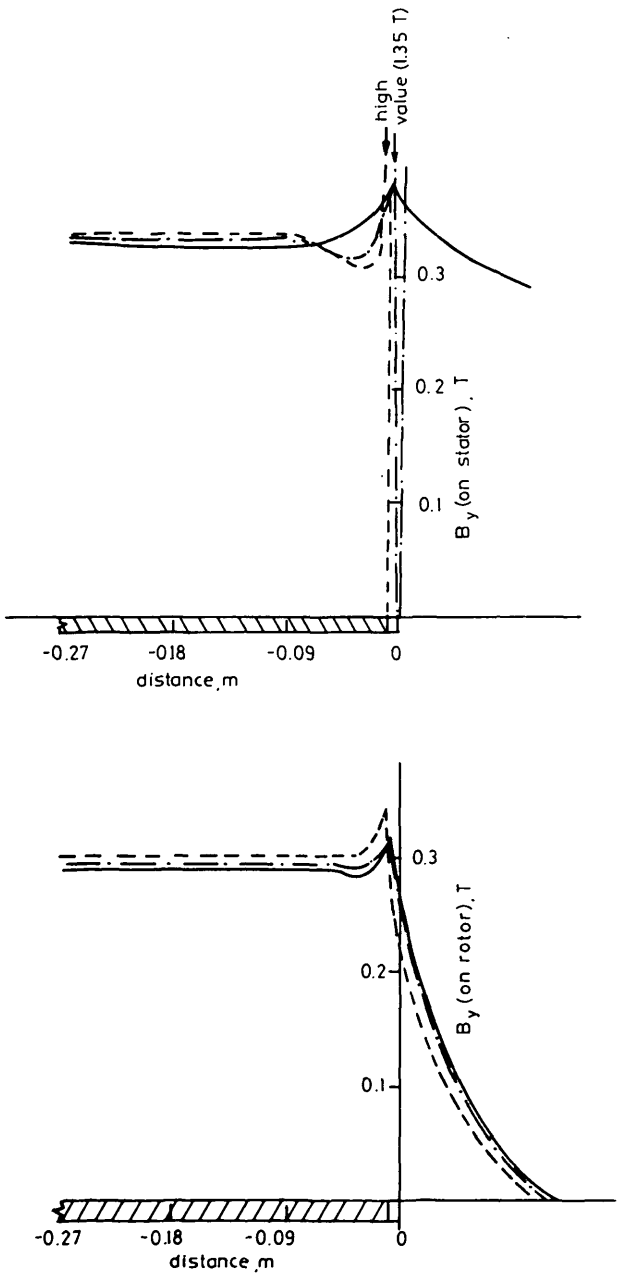


**Fig. 6** *Flux distribution due to exit-end effect (Motor A, 0.05 slip)*

– – – – stator without iron extension
– · – · – stator with a small iron extension
——— stator with infinite iron extension

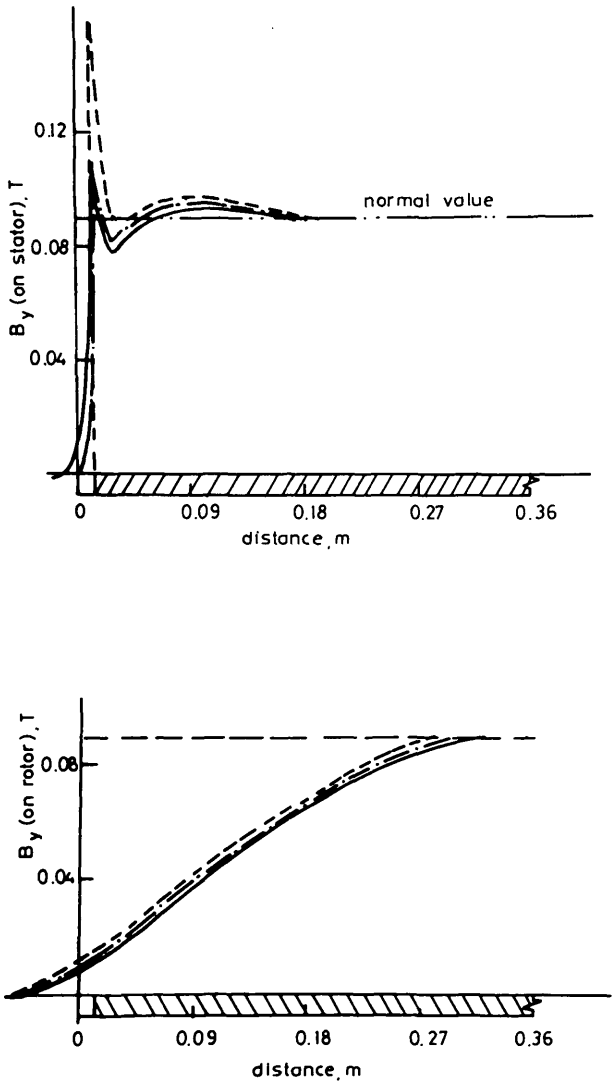


**Fig. 7** *Flux distribution due to entry-end effect (Motor A, 0.6 slip)*

– – – – stator without iron extension
– · – · – stator with a small iron extension
——— stator with infinite iron extension

this positive force considerably at low values of slip, including zero slip. However, even if a small amount of iron extension is present, this force reduces substantially.

For short stator lengths, particularly at small values of slip, the entry-end effect may last even up to the exit end. It is then necessary to consider the entry and exit-end effects simultaneously. As mentioned in Section 2, this leads to a 3-part mixed boundary value problem which can be solved by using an approximate Wiener-Hopf technique. Details of this method are given in Reference 12.

It can be seen from Fig. 5 that, for stator length equal to 0.36 m (four pole pitches) and for 0.05 slip, the entry-end effect does not decay completely at the exit end. Hence, simultaneous treatment of the end effects is required in this case. Fig. 11 gives the stator flux-density distribution obtained using such an analysis. For the same stator length, but at 0.6 slip, it can be seen from Figs. 7 and 8 that the end effects can be treated separately.

Finally, Figs. 12 and 13 compare results obtained by using 2-dimensional analysis with those obtained by 1-dimensional analysis. The 1-D treatment gives results which are close to those obtained by 2-D analysis, except that (i) it fails to predict the rotor flux density accurately, and (ii) it slightly overestimates the thrust.

In order to apply the analyses given so far to predict the performance of a practical machine, the following modifications are needed:

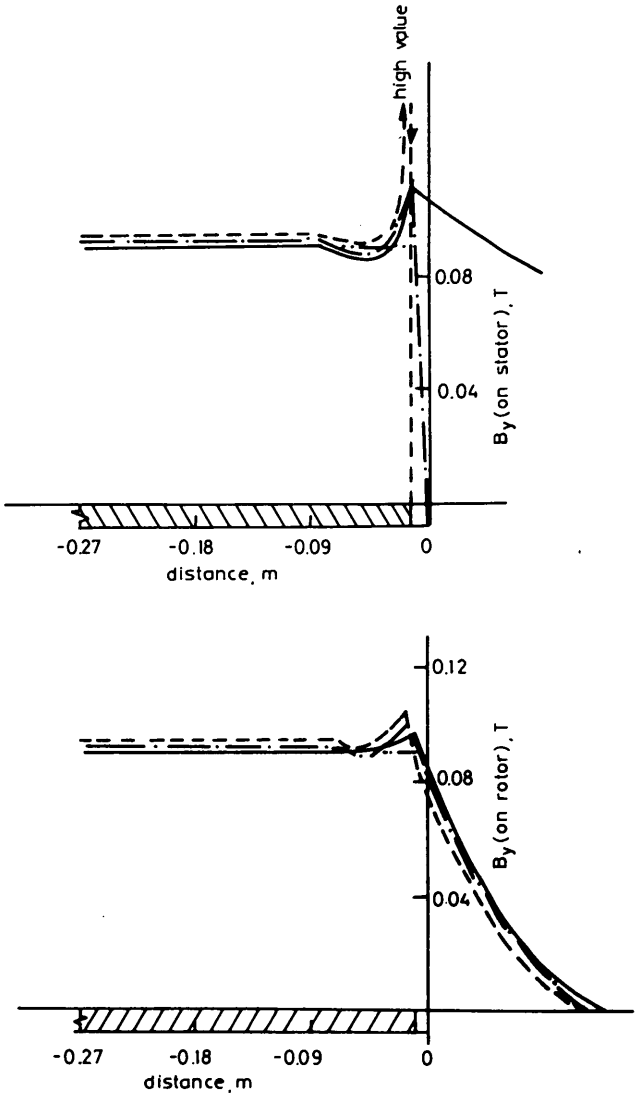


**Fig. 8** *Flux distribution due to exit-end effect (Motor A, 0.6 slip)*

– – – – stator without iron extension
– · – · – stator with a small iron extension
——— stator with infinite iron extension

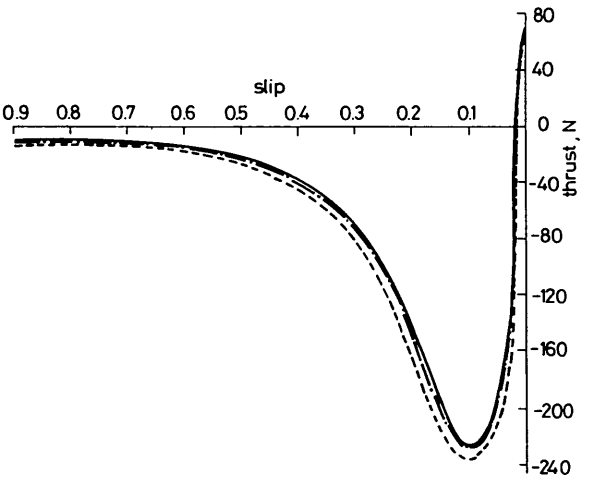


**Fig. 9** *Thrust due to entry-end effect (Motor A)*

– – – – stator without iron extension
– · – · – stator with 0.0124 m extension
——— stator with infinite iron extension

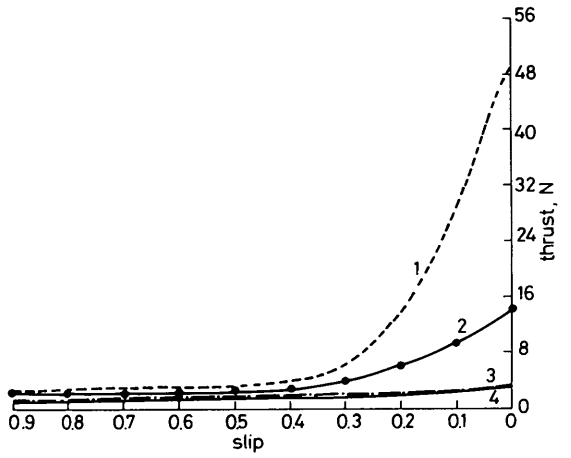


**Fig. 10** *Thrust due to exit-end effect (Motor A)*

– – – – stator without iron extension
—●—● stator with 0.003 m iron extension
– · – · – stator with 0.0124 m iron extension
——— stator with infinite iron extension

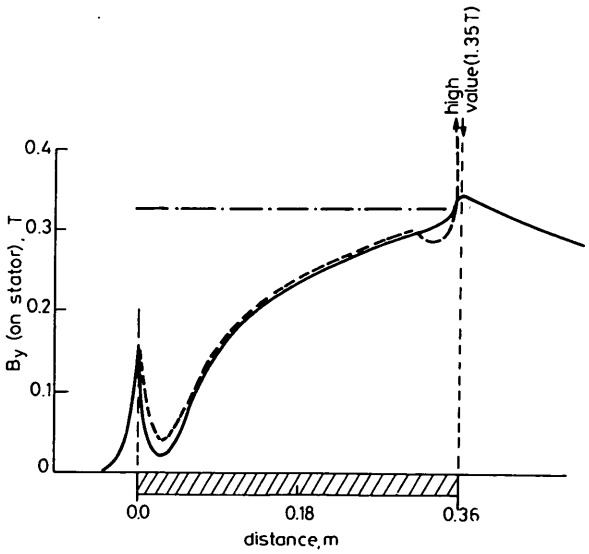


**Fig. 11** *Flux distribution on stator surface with simultaneous treatment of end effects (Motor A, 0.05 slip)*

– – – – stator without iron extension
——— stator with infinite iron extension
—— · —— without end effects

(i) The finite length effects in the transverse direction are to be taken into account by modifying the gap length and conductivity of the secondary sheet. It can be shown from Bolton's analysis [11, 13] that $g_{eff}$ and $\sigma_{eff}$ to be used in the 2-dimensional model are related with the true values by the following relation:

$$g_{eff} + \frac{j\sigma_{eff}\mu_0 ds\omega}{k^2} = \frac{g + (j\mu_0 s\omega d\sigma/k^2)}{1 + (\tanh rW_1/rW_1 Mg)(j\sigma\mu_0 ds\omega/k^2)} \quad (14)$$

where $s$ = slip, $r^2 = k^2 + (j\sigma\mu_0\omega ds/g)$, $M = 1 + (r/k)\tanh rW_1 \tanh k(W_2 - W_1)$, $2W_1$ = width of stator block, and $2W_2$ = width of rotor sheet.

(ii) In double-layer stator windings, the two layers are often staggered. The application of Wiener-Hopf technique to this situation does not offer any special difficulty.

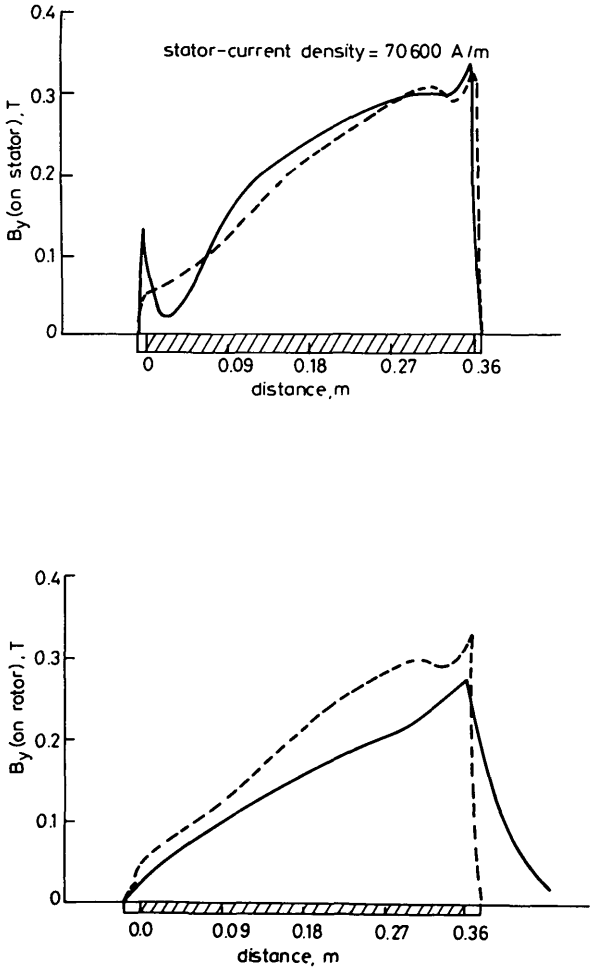


**Fig. 12** *Comparison of flux distributions by 1-D and 2-D analyses (Motor A, 0.05 slip)*

– – – – 1-D analysis
——— 2-D analysis

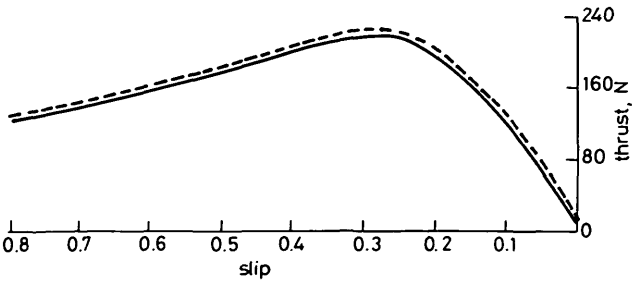


**Fig. 13** *Comparison of thrusts by 1-D and 2-D analyses*

– – – – 1-D analysis
——— 2-D analysis

(iii) The performance of the machine at constant applied voltage is to be computed from constant-current operation, taking into account the stator resistance and leakage reactance drops.

Incorporating the above modifications and making use of the 2-D analysis with simultaneous treatment of the end effects, the performance of the linear motor constructed and tested by Coho, Kliman and Robinson [10] is predicted at the operating condition of 100 V at 150 Hz. The flux-density distribution on the stator surface and in the yoke are predicted at 0.06 slip and are plotted in Fig. 14 along with the experimental results. The variation of the total thrust with slip is shown in Fig. 15, along with the test results. The correlation between the experimental and predicted values can be considered as satisfactory. Similar correlation was obtained for the operating condition of 40 V at 60 Hz. In predicting the results, a small amount of iron extension, as calculated from eqn. 6, is assumed to allow for fringing flux.

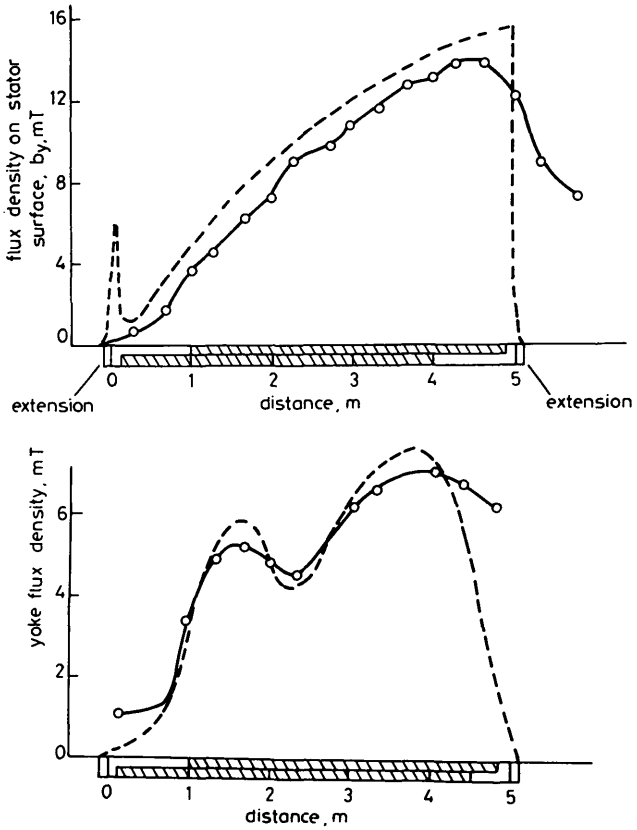


**Fig. 14** *Air gap and yoke flux distribution in motor of Reference 10 (100 V, 150 Hz, 0.06 slip)*

—o—o— test values
– – – predicted values

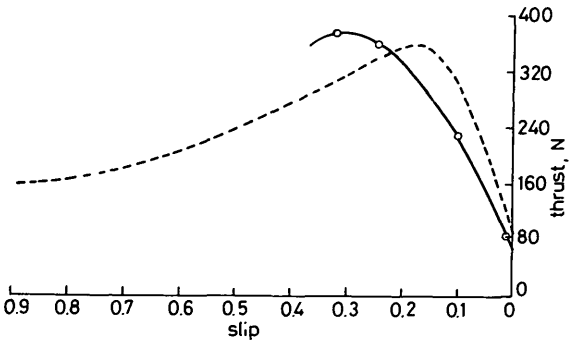


**Fig. 15** *Variation of thrust with slip (Motor of Reference 10; 100 V, 150 Hz)*

—o—o— test values
– – – predicted values

## 7 Conclusions

A 2-dimensional analysis is presented for a double-sided short stator LIM, taking into consideration the discontinuity in iron along with the discontinuity in the winding, using the Wiener Hopf technique. It is shown that discontinuity in the iron gives rise to peaking of flux density on the stator surface in a small region near the tips of the entry and exit ends. The effect is more pronounced at the exit end. Regarding forces, the discontinuity in the iron at the entry end gives rise to a small negative thrust, whereas at the exit end it gives rise to positive thrust which can reach appreciable values for small values of slip, including zero slip. However, all these effects are substantially reduced by even a small amount of iron extension.

From the overall results, it appears that the loss of thrust in a linear induction motor is almost entirely caused by the effect of discontinuity in the stator winding at the entry end. It is also desirable that there is no iron extension at the exit end.

## 8 Acknowledgments

The authors are grateful to Prof. N. Kesavamurthy, Head of the Electrical Engineering Department of IIT, Kharagpur, for his valuable suggestions and assistance rendered in revising the original MS of the paper. One of the authors (T.P.R.) wishes to express his sincere thanks to the authorities of the Regional Engineering College, Warangal for sponsoring him to carry out the work reported in this paper under the Quality Improvement Programme of the Government of India.

## 9 References

1 ITO, H., YAMAMURA, S., and ISHIKAWA, Y.: 'Theories of the linear induction motor and compensated linear induction motor', *IEEE Trans.*, 1972, **PAS-91**, pp. 1700–1710
2 BOLDEA, I., and NASAR, S.A.: 'Quasi-1-dimensional theory of linear induction motors with half-filled primary end slots', *Proc. IEE*, 1975, **122**, (1), pp. 61–66
3 DUKOWICZ, J.F.: 'Analysis of linear induction machines with discrete windings and finite iron length', *IEEE Trans.*, 1977, **PAS-96**, p. 66
4 NOBLE, B.: 'Methods based on the Wiener-Hopf technique for the solution of partial differential equations' (Pergamon Press, London, 1958)
5 COLLIN, R.E.: 'Field theory of guided waves' (McGraw-Hill, New York, 1960)
6 TITCHMARSH, E.C.: 'Theory of functions' (Oxford University Press, 1939, 2nd edn.)
7 YAMAMURA, S., ITO, H., and AHMED, P.: 'End effect of linear induction motor', *J. Inst. Electr. Eng. Jpn.*, 1968, **89**, pp. 459–469
8 NASAR, S.A.: 'Electromagnetic fields and forces in a linear induction motor, taking into account edge effects', *Proc. IEE*, 1969, **116**, (4), pp. 605–609
9 NASAR, S.A., and BOLDEA, I.: 'Linear motion electric machines', (Wiley, New York, 1976)
10 COHO, Q.C., KLIMAN, G.B., and ROBINSON, J.I.: 'Experimental evaluation of a high speed double sided linear induction motor', *IEEE Trans.*, 1975, **PAS-94**, pp. 10–17
11 BOLTON, H. 'Transverse edge effect in sheet-rotor induction motors', *Proc. IEE*, 1969, **116**, (5), pp. 725–731
12 VENKATARATNAM, K., and RAO, T.P.: 'Analysis of end effects in a short stator linear induction motor using approximate Wiener-Hopf technique'. Proceedings of the international conference on electrical machines, Pt. 1, Athens, Greece, 15th–17th Sept. 1980, pp. 50–59
13 RAO, T.P.: 'Two dimensional analysis of a short stator double sided linear induction motor using Wiener-Hopf technique'. Ph.D. thesis (Indian Institute of Technology, Kharagpur, WB, India), 1981

## 10 Appendixes

### *10.1 Wiender-Hopf techniques for the solution of $\psi_+$ and $\psi'_-$*

The first step in the solution of $\psi_+$ and $\psi'_-$ occurring in eqn. 5 is to write

$$\frac{f_1(s,g)}{f_2(s,g)} = \frac{G_-(s)}{G_+(s)}$$

where $G_-$ is regular in Re $s < b$, and $G_+$ is regular in Re $s > a$, $b > a > 0$ (Fig. 2). Knowing the zeros of $f_1(s, g)$ and $f_2(s, g)$, these can be expressed in their infinite product form as:

$$f_1(s,g) = f_1(0,g) \prod_{n=1}^{\infty} (1 - s/\alpha_n)(1 + s/\beta_n)$$

$$f_2(s,g) = f_2(0,g) \prod_{n=1}^{\infty} (1 - s/\gamma_n)(1 + s/\delta_n)$$

Hence

$$G_-(s) = f_1(0,g) \prod_{n=1}^{\infty} \frac{(1 - s/\alpha_n)}{(1 - s/\gamma_n)}$$

and

$$G_+(s) = f_2(0,g) \prod_{n=1}^{\infty} \frac{(1 + s/\delta_n)}{(1 + s/\beta_n)}$$

Assuming this is done, we can write eqn. 5*a* as:

$$\frac{\psi_+}{\psi'_- + \dfrac{J_0\mu_0}{s + jk}} = \frac{G_-}{G_+}$$

On rearranging, we get

$$\psi_+ G_+ = \psi'_- G_- + \frac{J_0\mu_0 G_-}{s + jk} \tag{15}$$

The LHS expression of eqn. 15 is regular in Re $s > a$. The first term on the RHS is regular in Re $s < b$, while the second term would have been regular in Re $s < b$, but for a pole at $s = -jk$. The second term can be resolved into the sum of $C_+(s)$ and $C_-(s)$, $C_+(s)$ being regular in Re $s > a$ and $C_-(s)$ being regular in Re $s < b$. Substituting and rearranging, eqn. 15 becomes

$$\psi_+ G_+ - C_+ = \psi'_- G_- + C_- \tag{16}$$

The LHS of eqn. 16 is defined and regular in Re $s > a$, and the RHS is defined and regular in Re $s < b$, both being regular in the common strip, $a <$ Re $s < b$. From the knowledge of the asymptotic behaviour of the individual terms of eqn. 16 and from Liouville's theorem of analytic continuation, it can be shown [13] that eqn. 16 is equal to zero. Thus,

$$\psi_+ = C_+/G_+ \qquad \text{and} \qquad \psi'_- = -C_-/G_-$$

### *10.2 Determination of $C_+$ and $C_-$*

The term $(J_0\mu_0)/(s + jk)$ is resolved into the sum of $C_+$ and $C_-$, using the method of partial fractions:

$$\frac{J_0\mu_0 G_-(s)}{(s + jk)} = C_+(s) + C_-(s)$$

$$= C_+(s) + \sum_n \frac{A_n}{(s - \gamma_n)}$$

Multiplying both sides by $(s - \gamma_n)$ and setting $s = \gamma_n$:

$$A_n = \left\{ \frac{J_0\mu_0}{(\gamma_n + jk)} (s - \gamma_n) G_-(s) \right\}_{s=\gamma_n}$$

$$= \frac{J_0\mu_0 G_-^{(R)}(\gamma_n)}{(\gamma_n + jk)}$$

where $G_-^{(R)}(\gamma_n)$ is the residue of $G_-(s)$ at $s = \gamma_n$. Hence,

$$C_-(s) = \sum_n \frac{J_0\mu_0 G_-^{(R)}(\gamma_n)}{(\gamma_n + jk)(s - \gamma_n)}$$

and

$$C_+(s) = \frac{J_0\mu_0 G_-(s)}{(s + jk)} - \sum_n \frac{J_0\mu_0 G_-^{(R)}(\gamma_n)}{(\gamma_n + jk)(s - \gamma_n)}$$